2016 American Control Conference (ACC)
Boston Marriott Copley Place
July 6-8, 2016. Boston, MA, USA

A Varying Frequency Resonant Control Strategy for Single Phase PWM Controlled Rectifiers

G. A. Ramos[1], J. A. Cifuentes[2] and I. D. Melo-Lagos[3]

Abstract— **Controlled PWM rectifiers are power electronic devices designed to diminish the harmonic pollution of electrical networks and intended as an answer to the power quality standards. Conventional proportional-integral controllers constitute a very useful technique to control these devices, however they do not exhibit high performance. Repetitive and resonant control have proven to be effective in this application under constant network frequency, but their performance decreases considerably under varying frequency conditions. In this work, we propose a varying frequency resonant control strategy that uses the measure of the network frequency for the on-line tuning of the control system resonant components. Stability analysis is carried out based on the LMI gridding approach and the experimental results show the effectiveness of the proposed strategy.**

I. INTRODUCTION

Power rectifiers are fundamental part of a vast variety of applications such that power inverters, uninterruptible power supplies (UPS), variable speed/frequency drives, switched power supplies, among others. However, these power devices are the major contributors to harmonic pollution in electrical distribution networks [1], [2]. Due to the constant expansion of these applications, power quality has been defined as a fundamental topic in which electrical system based its appropriate operation. Some standards related to power quality are IEC 1000-3-2 [3] and IEEE519 [4].

Pulse width modulation (PMW) controlled rectifiers raised as a strategy aimed at the reduction of harmonic pollution in electrical networks ([5], [6]) and as a solution to accomplish power quality standards [1]. The control objective is to obtain a sinusoidal current waveform in phase with the voltage network. This performance can be measured by means of the Total Harmonic Distortion (THD) and Power Factor (PF), the first one is used to quantify the presence of harmonics that degrade the shape of a signal and the latter to evaluate the phase shift between the current and voltage signals. Therefore, it is desirable to obtain a low THD with PF close to 1.

Proportional Integral (PI) controllers are commonly used in the rectifier current control since they imply a simple design and easy practical implementation [2]. However, the nature of this controller does not allow obtaining high performance [7].

Resonant control [2], [8], [9] and Repetitive Control (RC) [10], [11], [12] are control strategies designed to deal with periodic signals, i.e. they provide tracking and rejection of periodic references and disturbances. High performance controllers applied to power rectifiers have been reported in [5], [10]. The main drawback of these techniques is based on an important performance degradation when the frequency of the signals varies [13] which is a common fact in electrical networks.

In this work, a varying frequency resonant controller VFRES is proposed for the current control loop of a PWM controlled rectifier. This controller employs a Phase Looked Loop (PLL) to measure the network frequency and uses this information to tune each resonant component in the controller. As a result, the controller adjusts automatically the resonant frequency to match the frequency of the voltage network. Experimental results show very high performance at nominal frequency and performance preservation when the frequency of the network changes.

The article is organized as follows: Section II describes the PWM controlled rectifier and defines the control objectives, Section III presents the resonant control strategy and its design methodology as well as the variable frequency functionality. Experimental results are documented in Section IV and conclusions are presented in Section V.

II. PWM CONTROLLED RECTIFIER

A. System model

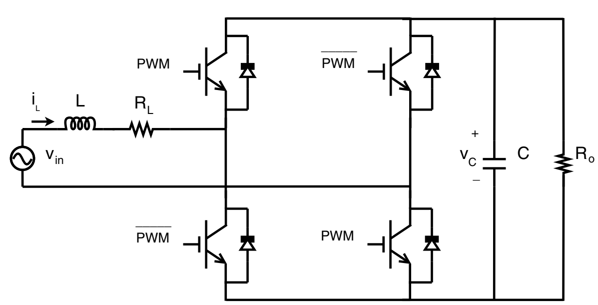

Fig. 1. Single-phase controlled rectifier.

Figure 1 shows the basic configuration of a PWM rectifier. The rectifier is connected to the ac voltage network and by means of a full bridge of controlled switches, a rectified voltage is obtained. The dynamic behavior of the rectifier

*This work was not supported by any organization

[1]G. A. Ramos is with the Department of Electrical and Electronic Engineering, Universidad Nacional de Colombia, Bogotá–Colombia garamosf@unal.edu.co
[2]J. A. Cifuentes is with the Department of Electrical and Electronic Engineering, Universidad Nacional de Colombia, Bogotá–Colombia jacifuentesq@unal.edu.co
[3]I. D. Melo is with PowerSun SAS, Bogotá–Colombia idmelol@unal.edu.co

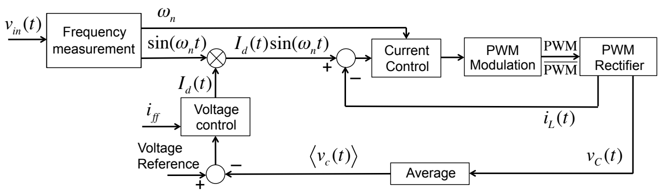

Fig. 2. Double loop control system structure.

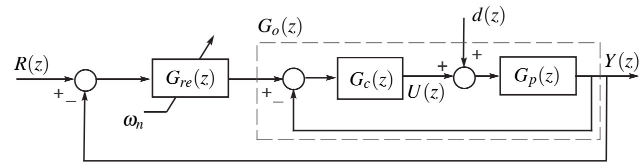

Fig. 3. Control Structure based on resonant elements.

can be expressed using the averaged model at the PWM switching frequency, resulting

$$\begin{array}{rcl} L\frac{di_L}{dt} + R_L i_L & = & v_{in} + d_c v_c \\ C\frac{dv_c}{dt} & = & d_c i_L - \frac{v_c}{R_o} \end{array} \tag{1}$$

where L is the inductance, R_L is the parasitic resistance of the inductance, i_L is the input current, C is the capacitance, v_C is the output voltage, R_o is the load resistance $v_{in} = V_{in}\sqrt{2}\sin(\omega_n t)$ is the ac voltage source and $\omega_n = 2\pi/T_p$ rad/s is the network frequency. The control action d_c is defined in the interval $[-1, 1]$.

B. Control Objectives

The control objective is to ensure an input current, $i_L(t)$, with sinusoidal shape in phase with the voltage source. This can be written as $i_L^* = I_d^* \sin(\omega_n t)$, where $x*$ represents the steady state of the signal $x(t)$. Hence, it is required that the control system tracks a sinusoidal signal of suitable magnitude, I_d, and rejects the disturbances. System disturbances are low frequency disturbances and harmonics introduced by the voltage network and dc output voltage. Harmonics in the voltage source are usually between the third and nine-nth component.

An additional control goal is to keep constant the averaged value of the output voltage. Therefore, it is needed that the system provides robustness against voltage network changes and load variations.

The control system scheme based on the objectives before mentioned is shown in Figure 2. The scheme has two control loops: the internal loop or current loop in charge of assuring a sinusoidal input current and the external loop or voltage loop by means of which the output voltage is regulated and also the active power balance is performed. The output of the later is the amplitude of the sinusoidal reference, I_d, that is sent to the current loop.

In this work, a current loop controller is proposed based on varying frequency resonant elements. This controller is designed to compensate the odd harmonics introduced by the voltage network as well to provide robustness against network frequency variations.

The voltage loop controller is a PI compensator that allows the active power balance and output voltage regulation.

III. CURRENT CONTROL LOOP

A. Resonant control

Resonant control is based on the Internal Model Principle (IMP) which establishes that in order to track/reject a exogenous signals, the model of those signals must be included in the control loop [14]. In this way, resonant controllers are designed to provide tracking/rejection of periodic signals. In order to do that, several models of sinusoidal signals, for a fundamental frequency and its harmonics, are added to the control loop. Therefore, tracking/rejection of periodic signals can be achieved by adding m resonant elements and these elements are selected according to the harmonic content of the signal. Each resonant element can be defined as:

$$R_l(z) = g_l \frac{\cos(\varphi_l) z^2 - \cos(\omega_l T_s + \varphi_l) z}{z^2 - 2\cos(\omega_l T_s) z + 1} \tag{2}$$

where g_l positive gain, φ_l is the phase shift of $R_l(z)$ at frequency ω_l and l defines the represented harmonic component. As shown in Figure 3, the structure of the resonant controller has two control loops. The internal loop is compound by the plant $G_p(z)$ and the controller $G_c(z)$ which is designed to provide enough robustness margins. The transfer function of the internal loop is $G_o(z) = G_c(z)G_p(z)/(1 + G_c(z)G_p(z))$. The external loop is defined by the following controller:

$$G_{re}(z) = R_0(z) + \sum_{l=1}^{m} R_l(z), \tag{3}$$

which is in charge of providing the tracking and rejection performance and has two parts:

1) $R_0(z)$ which provides low frequency performance. In this work it is assumed as a constant R_0.
2) A finite number of resonant elements $R_l(z)$ con $l = 1, \ldots, m$.

1) Tuning procedure: The tuning procedure seeks the selection of gains g_l and phase shifts φ_l in such a way that the controller achieves the desired performance with enough robustness margins. The procedure follows the ideas presented in [15].

The first step fixes the phase shifts φ_l to maximize de phase margins of the system while in the second step, gains g_l are selected to obtain the best possible performance with enough gain margins.

Figure 4 depicts the frequency response of a controller with 5 resonant elements tuned for a fundamental frequency of 60 Hz and the first 4 odd harmonics with a sampling frequency of 15 kHz. It can be seen, that the model provides infinite gain for the selected frequencies. This high gain allows the tracking/rejection properties of the closed loop system. From Figure 4, it can be concluded that a system with m resonant elements has m resonant peaks and $m - 1$ local minimums in its magnitude response, while the phase response has m discontinuities of $-\pi$ rad.

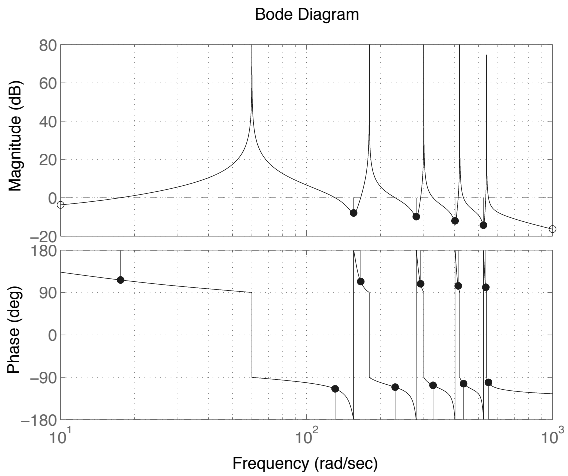

Fig. 4. Frequency response of a system with 5 resonant elements with fundamental frequency of 60 Hz. Marks: stability margins.

The first design key point is that the discontinuities of $-\pi$ rad given at each ω_l are centered in $-\varphi_l$. Given that the gain crossover frequencies are located besides the frequencies ω_l, it is desirable that the phase discontinuities are centered around 0° in order to obtain phase margins as large as possible.

The frequency response of the loop transfer function defined as $G_{loop}(z) = G_{re}(z)G_o(z)$, is obtained from the response of the resonant elements $G_{re}(z)$ (see Figure 4) modified by the internal loop $G_o(z)$. Hence, to obtain the largest phase margins it is necessary to cancel out the phase of $G_o(z)$ at each resonant frequency. This can be achieved defining the phase shift of each resonant element as $\varphi_l = \arg\left(G_o(e^{j\omega_l T_s})\right)$, which ensures that the open loop phase of $G_{loop}(z) = G_{re}(z)G_o(z)$ is zero at each frequency ω_l.

The second design key point is that the phase changes of ±180° occurs in the vicinity of the local minimums (see Figure 4). As a consequence, the crossover phase frequencies are located close to the local minimums frequencies and the gain margins are calculated at those frequencies. Additionally, the local minimums are defined by the gain of adjacent resonant elements. Therefore, to preserve stability robustness, the gains of the resonant elements should be selected in order to locate the local minimums under the 0 dB. At the same time, gains g_l should be the maximum possible to guarantee high enough performance.

Figure 4 shows the result of the tuning procedure for the PWM controlled rectifier under study.

B. Variable frequency operation

From Figure 4 it can be observed that each resonant element provides high gain in a very selective manner and this characteristic is the main disadvantage of this models in case of varying frequency. In this way, when the frequency of the exogenous signal deviates from the nominal one, the resonant controller losses the high gain and the performance is degraded [16]. In the rectifier application, it is a fact that the network frequency varies in time and these variations can be large for weaker networks as in rural areas.

To overcome this issue, an adaptation system is proposed in which the frequency of the source is injected to each resonant element in order to match the resonant and network frequencies. Network frequency is calculated using a PLL and the information is passed to the resonant controller. This allows maintaining the steady state performance of the controller under varying frequency conditions.

1) Stability: The stability analysis is based on the state-space representation of the closed loop system of Figure 3 and the resonant elements definition, equations (2) and (3). Thus, given the state-space representation of $G_o(z)$:

$$\begin{aligned} \mathbf{x}_o(k+1) &= \mathbf{A}_o\mathbf{x}_o(k) + \mathbf{b}_o u(k) \\ y(k) &= \mathbf{c}_o\mathbf{x}_o(k) \end{aligned}$$

and representation of controller $G_{re}(z)$:

$$\begin{aligned} \mathbf{x}_{re}(k+1) &= \mathbf{A}_{re}(\bar{\omega})\mathbf{x}_{re}(k) + \mathbf{b}_{re}e(k) \\ u(k) &= \mathbf{c}_{re}(\bar{\omega})\mathbf{x}_{re}(k) + \mathbf{d}_{re}e(k) \end{aligned}$$

with $\bar{\omega} \in [\bar{\omega}_{min}, \bar{\omega}_{max}]$ the frequency measured by the PLL and injected to the resonant controller delimited by the interval $\bar{\omega}_{min}$ y $\bar{\omega}_{max}$, being

$$\mathbf{A}_{re}(\bar{\omega}) = \begin{bmatrix} \mathbf{A}_m(\bar{\omega}) & \mathbf{0} & \cdots & \mathbf{0} & \mathbf{0} \\ \mathbf{0} & \mathbf{A}_{m-1}(\bar{\omega}) & \cdots & \mathbf{0} & \mathbf{0} \\ \vdots & \vdots & \ddots & \vdots & \vdots \\ \mathbf{0} & \mathbf{0} & \cdots & \mathbf{A}_2(\bar{\omega}) & \mathbf{0} \\ \mathbf{0} & \mathbf{0} & \cdots & \mathbf{0} & \mathbf{A}_1(\bar{\omega}) \end{bmatrix},$$

$$\mathbf{b}_{re} = \begin{bmatrix} \mathbf{b}_m \\ \mathbf{b}_{m-1} \\ \vdots \\ \mathbf{b}_2 \\ \mathbf{b}_1 \end{bmatrix},$$

$$\mathbf{c}_{re}(\bar{\omega}) = \begin{bmatrix} \mathbf{c}_m(\bar{\omega}) & \mathbf{c}_{m-1}(\bar{\omega}) & \cdots & \mathbf{c}_2(\bar{\omega}) & \mathbf{c}_1(\bar{\omega}) \end{bmatrix},$$

$$\mathbf{d}_{re} = \sum_{l=1}^{m} d_l + R_0$$

which are defined by the matrices of each resonant element:

$$\mathbf{A}_l(\bar{\omega}) = \begin{bmatrix} 2\cos(\bar{\omega}_l T_s) & -1 \\ 1 & 0 \end{bmatrix}, \mathbf{b}_l = \begin{bmatrix} 1 \\ 0 \end{bmatrix},$$

$$\mathbf{c}_l = g_l \begin{bmatrix} -\cos(\bar{\omega}_l T_s + \varphi_l) + 2\cos(\bar{\omega}_l T_s)\cos(\varphi_l) & -\cos(\varphi_l) \end{bmatrix},$$

$$\mathbf{d}_l = g_l\cos(\varphi_l)$$

being l the related harmonic number. The closed loop system of Figure 3 accepts the following state-space representation:

$$\begin{aligned} \mathbf{x}(k+1) &= \mathbf{A}(\bar{\omega})\mathbf{x}(k) + \mathbf{b}r(k) \\ y(k) &= \mathbf{c}\mathbf{x}(k) + \mathbf{d}r(k) \end{aligned} \tag{4}$$

where

$$\mathbf{A}(\bar{\omega}) = \begin{bmatrix} \mathbf{A}_o - \mathbf{b}_o\mathbf{c}_o\mathbf{d}_{re} & \mathbf{b}_o\mathbf{c}_{re}(\bar{\omega}) \\ -\mathbf{b}_{re}\mathbf{c}_o & \mathbf{A}_{re}(\bar{\omega}) \end{bmatrix},$$

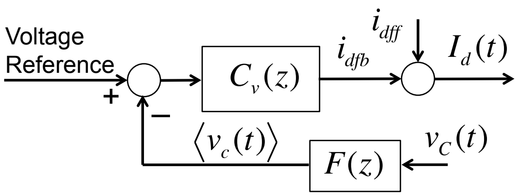

Fig. 5. Voltage loop structure.

$$\mathbf{b} = \begin{bmatrix} \mathbf{b}_o \mathbf{d}_{re} \\ \mathbf{b}_{re} \end{bmatrix}, \mathbf{c} = \begin{bmatrix} \mathbf{c}_o & \mathbf{0} \end{bmatrix}$$

As a result, given $\mathbf{b}$ and $\mathbf{c}$ bounded, stability of the closed loop system (4) can be established by means of the existence of a positive definite matrix $\mathbf{P}$ for which the following matrix inequality holds [17]:

$$Lyap(\mathbf{P}) := \mathbf{A}^T(\bar{\omega})\mathbf{P}\mathbf{A}(\bar{\omega}) - \mathbf{P} < 0 \tag{5}$$

However, (5) implies an infinite number of inequality given by the points in the interval of $\bar{\omega}$. To tackle this problem, we can use the Linear Matrix Inequalities (LMI) gridding approach [18], [19]. In this way, we can check the existence of matrix $\mathbf{P}$ for a uniformly distributed number of points in the interval $[\bar{\omega}_{min}, \bar{\omega}_{max}]$ and then using the obtained matrix, verify the stability for a denser set of points in the interval. This allows to infer the system stability for the points in the interval. However, this entails a necessary but not sufficient stability condition.

C. Voltage loop

Voltage loop control is designed to achieve an active power balance in the rectifier and to provide the magnitude of the current reference for the current loops. Given that voltage, at rectifier output terminal, has a waveform that is highly rippled, a low pass filter is usually applied to obtain a smoother signal. The purpose of this is to avoid the ripple propagation to the current reference $i_d(t)$, which would negatively impact the harmonic distortion of the rectifier input current $i_L(t)$. In this work, the low pass filter has been replaced by an averaging filter tuned at 60 Hz:

$$F(z) = \frac{1}{N}\frac{1 - z^{-N}}{1 - z^{-1}}$$

where $N = 250$. By using this filter, the average voltage is calculated from the output voltage as $V_{dc} = \langle v_c \rangle$.

Voltage loop structure is shown in Figure 5. This structure comprises two basic components: a feedback control action, i_{dfb}, generated by a PI compensator and a pre-feeding action i_{dff}. The PI controller in the feedback loop will regulate the average value of the output voltage to the desired value with zero error:

$$C_v(z) = k_i \frac{T_s}{2}\frac{z+1}{z-1} + k_p \tag{6}$$

On the other hand, the pre-feeding signal, i_{dff}, is designed in order to avoid that sudden changes in voltage levels cause transients with high current peaks. This pre-feeding stage is calculated based on the rectifier power balance in steady state. In this way, the balance between the AC active power and the DC power is given by:

$$\frac{1}{2}V_m I_m = V_{dc} I_{dc} + P_{losses}$$

where $V_m = V_{in}\sqrt{2}$ is the peak value of the network voltage, $I_m = I_d$ is the peak value of the rectifier input current, $V_{dc} = \langle v_c \rangle$ is the average value of the capacitor voltage, $I_{dc} = \langle i_L \rangle$ is the average value of the load current and P_{losses} are the rectifier losses. On that basis, the pre-feeding value can be computed by:

$$i_{dff} = \frac{1}{2}\frac{V_m I_m}{V_{dc}} + I_{losses}$$

where I_{losses} is a factor that weighs the rectifier losses. As a result, the reference signal amplitude for the current loop is calculated by:

$$I_d = i_{dfb} + i_{dff}$$

TABLE I
SELECTED PARAMETERS FOR THE RESONANT CONTROLLER

ω_l	$2\pi 60$	$2\pi 180$	$2\pi 300$	$2\pi 420$	$2\pi 540$
g_l	0.07768	0.02695	0.01638	0.01182	0.00929
φ_l	-3.642	-11.026	-18.205	-25.113	-31.686

IV. EXPERIMENTAL RESULTS

The utility network frequency is $f = 60$ Hz, defining a period $T_p = 1/60$ s. The sampling period are set to $T_s = 1/15000$ s which corresponds with the PMW switching frequency. The transfer function of the plant is obtained from (1) performing a variable change $\alpha = dv_c$, resulting

$$G_p(z) = \frac{1}{sL + R_L} = \frac{I_L(z)}{\alpha(z)} \tag{7}$$

From the discretization of (7), it is obtained:

$$G_p(z) = \mathscr{Z}\left[\frac{1}{sL + R_L}\frac{1 - e^{-T_s}}{s}\right]_{T_s}$$

with inductance $L = 600$ mH and parasitic resistance $R_L = 0{,}2$ ohms. The design is based on the structure of Figure 3. For the internal loop, the controller $G_c(z) = (-3.333z + 3.328)/(z - 0.998)$ provides enough robustness margins. For the external loop, the proportional controller is $R_0 = 0.1$ followed by 5 resonant elements ($m = 5$) tuned at fundamental nominal frequency of 60 Hz and its 4 first odd harmonics. The phase shift is defined as $\varphi_l = \arg\left(G_o(e^{j\omega_l T_s})\right)$. Gains g_l are selected to obtain good performance maintaining the robustness margins. Table I shows the designed gains g_l and phases φ_l for each resonant element and frequency ω_l.

The open loop response of the transfer function $G_{loop}(z) = G_{re}(z)G_o(z)$ is shown in Figure 4. It can be observed that the magnitude of the peaks decreases as the frequency increases. Furthermore, at each harmonic frequency, the phase change of $G_{loop}(z)$ is centered at 0 degrees which corresponds with the design of φ_l.

The PI controller for the voltage loop defined in (6) is tuned with $k_p = 0{,}01$ and $ki = 0{,}7$. An autotransformer is

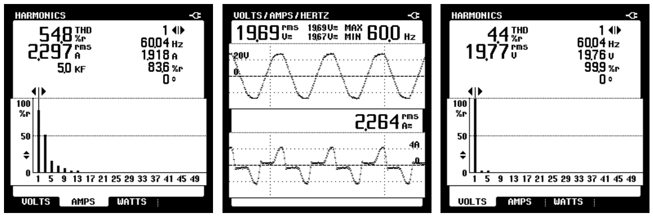

Fig. 6. Resulted waveforms for the non-controlled rectifier. Left: current harmonics, center: voltage and current waveforms, right: voltage harmonics

connected to the mains in order to provide $V_{in} = 20$ Vrms to the rectifier. The single-phase rectifier is a power converter from Semikron and control algorithms are implemented in an Intel PC with Matlab XPCTarget real time software. Bus dc voltage is Vc=36 V with resistive load of 25 ohms.

A. *Nominal frequency performance*

Figure 6 shows the response of a non-controlled rectifier. It can be observed a non-sinusoidal current waveform and its harmonic content for which a $THD = 54,8\%$ is obtained. Additionally, Figure 6 presents the voltage waveform and its harmonic content with the 3th and 5th harmonics. This distortion in the voltage network acts as a disturbance signal for the current control loop.

Figure 7 presents the results of the resonant controller at the nominal frequency of 60 Hz. It can be noticed that the controller exhibits a remarkable performance with $THD = 0.9\%$ and PF=1.

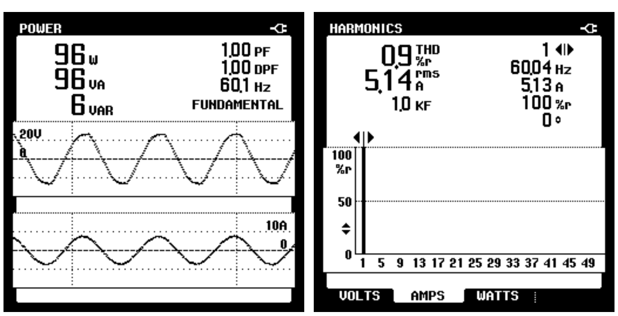

Fig. 7. Current waveform and harmonic content for the resonant controller at nominal frequency. left: waveform, right: harmonics.

B. *Variable frequency performance*

This set of experiments compare the varying frequency resonant controller (VFRES) with the same resonant controller but with fixed frequency (RES).

The stability analysis is performed using the LMI gridding approach described in Section III-B.1. Since the expected variation interval is about 1 Hz (for urban distribution networks), it is defined $\bar{\omega} \in [59.5, 60.5]$ Hz. Matrix $\mathbf{P}$ is found from equation (5) for 40 point uniformly distributed in the variation interval and other 500 points in the interval are used to verify the inequality. Figure 8 shows the maximum eigenvalue corresponding to equation (5). As a consequence, stability can be inferred for the given variation interval and also for frequencies in $\bar{\omega} \in [59.23, 60.76]$.

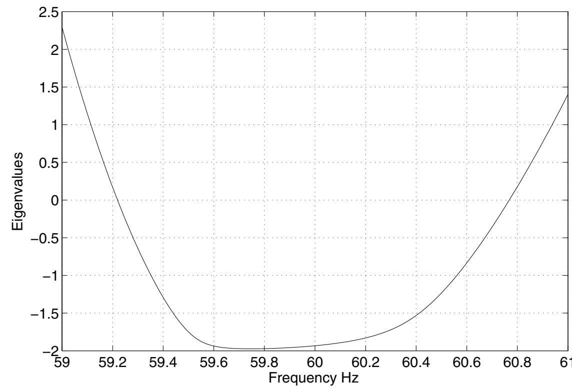

Fig. 8. Maximum eigenvalue corresponding to equation (5).

Since the network frequency is not a parameter that can be modified systematically, the experiments were carried out tuning both resonant controllers (VFRES and RES) at slightly different frequency, in this case $f = 60,3$ Hz.

Figure 9 shows the performance obtained with the controller VFRES and RES. It can be seen that controller RES losses its nominal performance with a THD of 2.3%. On the other hand, controller VFRES successfully adapts its resonant elements to the new frequency value and preserves the nominal performance with $THD = 0.9\%$, thus providing robustness against network frequency variations.

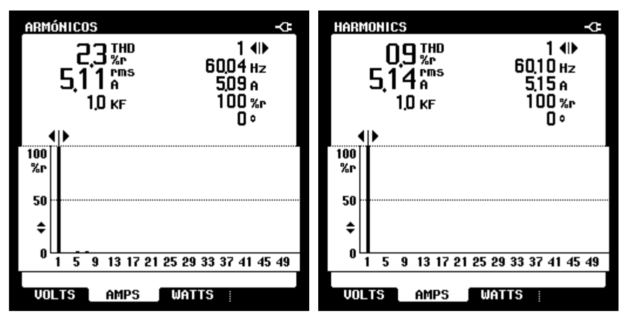

Fig. 9. Current harmonic content. left: fixed frequency resonant controller RES and right: varying frequency resonant controller VFRES.

Figure 10 shows the frequency measurement provided by the PLL for controller VFRES. As it can be noticed, small network frequency changes took place during experiments.

V. CONCLUSIONS

This article has proposed the use of a varying frequency resonant controller in the current control loop of a single-phase controlled rectifier. Simulations results have shown that the proposed controller achieves excellent performance with a THD of 0.9% and unitary power factor. The main advantage on the proposal against other high performance controllers is that the controller can follow the network frequency variations in order to maintain the steady state nominal performance.

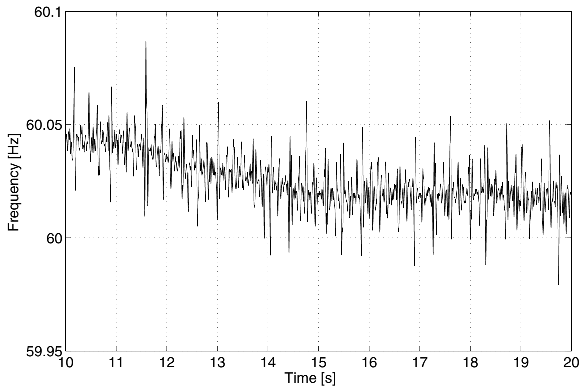

Fig. 10. PLL frequency estimation in controller VFRES.

ACKNOWLEDGMENT

This work is partially financed by the División de Investigación Sede Bogotá (DIB) of the Universidad Nacional de Colombia under the program Programa Nacional de Proyectos para el Fortalecimiento de la Investigación, la Creación y la Innovación en Posgrados de la Universidad Nacional de Colombia 2013 - 2015 with code Hermes 19348.

REFERENCES

[1] S. Bhattacharyya, J. Cobben, and W. Kling, "Harmonic current pollution in a low voltage network," in *Power and Energy Society General Meeting, 2010 IEEE*, July 2010, pp. 1–8.

[2] F. Li, Y. Zou, W. Chen, and J. Zhang, "Comparison of current control techniques for single-phase voltage-source pwm rectifiers," in *Industrial Technology, 2008. ICIT 2008. IEEE International Conference on*, April 2008, pp. 1–4.

[3] A. Prudenzi, U. Grasselli, and R. Lamedica, "Iec std. 61000-3-2 harmonic current emission limits in practical systems: need of considering loading level and attenuation effects," in *Power Engineering Society Summer Meeting, 2001*, vol. 1, 2001, pp. 277–282 vol.1.

[4] "Ieee recommended practices and requirements for harmonic control in electrical power systems," *IEEE Std 519-1992*, pp. 1–112, April 1993.

[5] R. Etz, T. Patarau, and D. Petreus, "Comparison between digital average current mode control and digital one cycle control for a bridgeless pfc boost converter," in *Design and Technology in Electronic Packaging (SIITME), 2012 IEEE 18th International Symposium for*, Oct 2012, pp. 211–215.

[6] J. Rodriguez, J. Dixon, J. Espinoza, J. Pontt, and P. Lezana, "Pwm regenerative rectifiers: state of the art," *Industrial Electronics, IEEE Transactions on*, vol. 52, no. 1, pp. 5–22, Feb 2005.

[7] Z. Shuai, A. Luo, C. Tu, and D. Liu, "New control method of injection-type hybrid active power filter," *Power Electronics, IET*, vol. 4, no. 9, pp. 1051–1057, November 2011.

[8] H.-S. Song, R. Keil, P. Mutschler, J. van der Weem, and K. Nam, "Advanced control scheme for a single-phase pwm rectifier in traction applications," in *Industry Applications Conference, 2003. 38th IAS Annual Meeting. Conference Record of the*, vol. 3, Oct 2003, pp. 1558–1565 vol.3.

[9] W. Helin, C. Qiming, L. Ming, C. Gen, and D. Liang, "The study of single-phase pwm rectifier based on pr control strategy," in *Control and Decision Conference (2014 CCDC), The 26th Chinese*, May 2014, pp. 3818–3823.

[10] C. Wang, Y. Zou, Y. Zhang, Y. Xu, X. She, and F. Li, "Research on the single-phase pwm rectifier based on the repetitive control," in *Industrial Technology, 2008. ICIT 2008. IEEE International Conference on*, April 2008, pp. 1–6.

[11] R. W. Longman, "Iterative learning control and repetitive control for engineering practice," *International Journal of Control*, vol. 73, no. 10, pp. 930–954, 2000. [Online]. Available: http://www.tandfonline.com/doi/abs/10.1080/002071700405905

[12] M. Tomizuka, "Dealing with periodic disturbances in controls of mechanical systems," *Annual Reviews in Control*, vol. 32, no. 2, pp. 193 – 199, 2008. [Online]. Available: http://www.sciencedirect.com/science/article/pii/S1367578808000321

[13] M. Steinbuch, "Repetitive control for systems with uncertain period-time," *Automatica*, vol. 38, no. 12, pp. 2103 – 2109, 2002. [Online]. Available: http://www.sciencedirect.com/science/article/pii/S0005109802001346

[14] B. Francis and W. Wonham, "Internal model principle in control theory," *Automatica*, vol. 12, pp. 457–465, 1976.

[15] M. F. Byl, S. J. Ludwick, and D. L. Trumper, "A loop shaping perspective for tuning controllers with adaptive feedforward cancellation," *Precision Engineering*, vol. 29, no. 1, pp. 27 – 40, 2005. [Online]. Available: http://www.sciencedirect.com/science/article/pii/S0141635904000546

[16] G. Ramos and R. Costa-Castelló, "Power factor correction and harmonic compensation using second-order odd-harmonic repetitive control," *Control Theory Applications, IET*, vol. 6, no. 11, pp. 1633–1644, July 2012.

[17] W. Rugh, *Linear system theory, 2nd Ed.* Prentice-Hall, Inc., Upper Saddle River, NJ, 1996.

[18] A. Sala, "Computer control under time-varying sampling period: An lmi gridding approach," *Automatica*, vol. 41, no. 12, pp. 2077 – 2082, 2005. [Online]. Available: http://www.sciencedirect.com/science/article/pii/S0005109805002190

[19] J. Olm, G. Ramos, and R. Costa-Castelló, "Stability analysis of digital repetitive control systems under time-varying sampling period," *Control Theory Applications, IET*, vol. 5, no. 1, pp. 29–37, January 2011.